行政院國家科學委員會專題研究計畫　成果報告

新世代鐵電非揮發性記憶元件(3/3)

計畫類別：個別型計畫
計畫編號：NSC92-2215-E-009-016-
執行期間：92 年 08 月 01 日至 93 年 07 月 31 日
執行單位：國立交通大學電子工程學系

計畫主持人：曾俊元

報告類型：完整報告

處理方式：本計畫涉及專利或其他智慧財產權，1 年後可公開查詢

中　華　民　國 93 年 11 月 2 日

新世代鐵電非揮發性記憶元件(3/3)

"Studies on next generation ferroelectric memory"

計畫編號：NSC92-2215-E-009-016

執行期間：92 年 8 月 1 日 至 93 年 7 月 31 日

主持人：曾俊元 交通大學電子工程系教授

摘要

近年來，關於使用鋇鍶鈦奈米薄膜(BST nano film)的多重添加製程所製作的電容式元件由於可以降低其操作時的介電損失(Dielectric loss)，增強操作時的介電可調致性能(Dielectric tunabilities)，所以被廣泛的加以討論與研製，此外相較於MOS元件上的鐵電記憶元件應用方面，鋇鑭鈦薄膜(BLT nano film)也因為具備著耐久度高與漏電流低同時驅動電壓小的優勢，而被積極的研究，本計劃的重點專注於探討這兩個極具潛力之材料的前瞻性製程，以鋇鍶鈦奈米薄膜而言，我們發現添加銀進入薄膜中將可以同時提升介電可調致性約 1%及降低介電損失達 0.005，另外在鋇鑭鈦薄膜的MFIS結構應用上，已經可以成功製作奈米等級的薄膜，其奈米晶粒的最佳堆積使得其漏電流機制得到一定程度的抑制，漏電流可以維持在 10^{-7} A/cm^{3}左右，同時在CV的量測上正負壓降所可以驅動的偏移範圍(memory windows)在操作電壓 5V時約可以達到 1.2 V附近，極具有商業應用的潛力。

關鍵字: 鐵電記憶體元件, 鋇鍶鈦氧化物及鉍鑭鈦氧化物

1. Abstract

The new material, Ag-BST, was investigated for the metal-insulator-metal (MIM) structure. Nanocrystalline $Ba_{0.5}Sr_{0.5}TiO_3$ (BST) and Ag doped $Ba_{0.5}Sr_{0.5}TiO_3$ (Ag-BST) composite thin films were deposited on Pt/Ti/SiO_2/Si substrates by a sol-gel method. The capacitance-voltage (*C-V*) characteristics indicated a reduction in capacitance and a slight shift in the *C-V* maxima for Ag(1)-BST (~+0.1 V) and Ag(2)-BST (~+0.2 V) films when measured down field for the series configuration involving low dielectric interface layers and asymmetric distribution of charge carriers in the films. Dielectric tunabilities of pure BST (21% ± 2%) and Ag(1)-BST (22% ± 2%) were comparable and that of Ag(2)-BST was ~15% ± 2% with a broadened *C-V* maximum. The dielectric loss (tan δ) at zero bias voltage decreased in the order of BST (0.025 ± 0.001) > Ag(1)-BST (0.020 ± 0.001) > Ag(2)-BST (0.018 ± 0.001) and remained unchanged in the entire range of measurement (-6 ↔ +6 V) for Ag(2)-BST due to the dense microstructure, low relaxational loss, and enhanced polarization pinning. Moreover, the metal/ferroelectric/insulator/ semiconductor (MFIS) was studied for the application in the integrated circuit. The sol-gel derived ferroelectric $Bi_{3.25}La_{0.75}Ti_3O_{12}$ (BLT) and rf-sputtered insulator TiO_2 films for the application in the MFIS structure were investigated in the present study. The X-ray diffraction and electrical analysis results show that the TiO_2 insulator layer plays an important role of not only the template for growing highly oriented BLT films but also the diffusion barrier between BLT and Si interface. The memory windows of the MFIS structure measured by the capacitor-voltage method were in the range of 0.2 to 1.2 V while the gate voltage varied from 2 to 5 V. The MFIS structure of Pt/ 200 nm BLT/ TiO_2/ Si is expected to be suitable for nondestructive read-out ferroelectric random access memory applications.

Key word: Ferroelectric memory, BST, BLT and MFIS

2. Introduction

There had been interest in the past several

decades to discover the silver (Ag) affects on modifying the microstructure and resultant physical properties.[1] Recently, the pulsed- laser-deposited (PLD) Ag-BST thin films[2] exhibited higher capacitance for 5 wt % Ag-doped samples, which was ascribed to the improved oxygenation of the BST film, as metastable silver oxide phases decomposed during the thermal processing of the film and filled the oxygen vacancies. However, no dielectric loss characteristics were discussed. In this study, the effect of Ag addition on the capacitance and characteristics of sol-gel derived BST thin films was carrying out.

Ferroelectric material, such as BLT, with high dielectric constant is widely applied for ferroelectric memory.[3] The main challenges of ferroelectric materials for memory are good capacitive properties, simple fabrication and long retention. Based on all these issues, BLT in MFIS structure is expected to be used in ferroelectric memory applications. Therefore, the capacitance properties of Pt/BLT/TiO_2/Si structure were also discussed.

3. Experimental procedure

The BST and 1 mole% and 2 mole% Ag doping–BST (Ag(1)–BST and Ag(2)–BST) thin films were prepared by an acetate precursor sol-gel route. Stoichiometric amounts of the precursor materials were $Ba(OAc)_2$, $Sr(OAc)_2$, Ag(OAc) and $Ti(i–OPr)_4$ (OAc–Acetate, i–OPr–Isopropoxide) dissolved in acetic acid and ethylene glycol solution. This thin films were spin–coated on Pt (100 nm)/Ti(5 nm)/SiO_2 (500 nm)/Si substrates, and pyrolyzed at 200 ^oC and finally annealed at 700 ^oC for 2h in air.

For the MFIS structure, a 10-nm-thick SiO_2 and TiO_2 gate dielectrics were deposited on Si. Then BLT was deposited on SiO_2/Si and TiO2 /Si by sol-gel method. The BLT precursors were prepared from bismuth acetate, lanthanum acetate hydrate, and titanium n-butoxide, which were dissolved in the solvent composed of acetic acid, 2-methoxythanol, and glycerol in sequence. After the spin coating deposition, the films were pyrolyzed and rapid thermal annealed at 650 °C for 1 h.

4. Results

Figure 1 shows the XRD patterns of BST, Ag(1)-BST and Ag(2)-BST films. All the diffraction peaks are indexed to BST phase with (200) prefer orientation. The reduction in intensities of diffraction peaks of Ag(1)-BST and Ag(2)-BST were caused by an increase in the degree of disorder in the orientation of the crystallites caused by Ag.

Figure 2 depicts the SEM analysis of the surface morphologies of BST, Ag(1)-BST and Ag(2)-BST films and cross-section for Ag(2)-BST film. The average grain size (d_{SEM}) of 27 nm uniform agglomerated on the BST film (Fig. 2a). An increase in nonuniformity was observed in Ag(1)-BST film with the d_{SEM} of 40 nm (Fig. 2b). For the Ag(2)-BST film, the agglomerate size (d_{SEM} ~25 nm) is highly uniform with no large ones observed. The microstructure is better than pure BST and Ag(1)-BST with considerable reduction in porosity (Figure 2c), which could be due to the low solubility of Ag in BST grains and its increased presence along the grain boundaries. The dense microstructure of Ag(2)-BST is further demonstrated by a cross-sectional SEM picture as shown in Fig. 2d.

The *C-V* curves of BST, Ag(1)-BST and Ag(2)-BST films are presented in Figure 3. The *C-V* curve for BST under increasing and decreasing field has identical position for maximum capacitance (C_m). No broadening of the *C-V* curve is observed for Ag(1)-BST despite a reduction in capacitance relative to BST and a slight positive shift (~ +0.1 V) of the C_m in the down field. For the Ag(2)-BST film, the *C-V* curve broadens and is associated with lowering and shifting of the C_m to ~ +0.2 V in the down field. It is interesting to note that the tunability of the *C-V* curve for Ag(1)-BST film (22 ± 2%) is comparable or marginally higher than BST (21 ± 2%). That the 1 mole % Ag addition improves the densification of the BST nanograins forming large agglomerates (Figure 2b) is due to the microstructure. The large agglomerates may have grains with identical polarization behavior causing an increase in polarization density, which results in the observed dielectric tunability being equal or marginally better than BST. The significant broadening of the capacitance with a reduction in tunability (15 ± 2%) for Ag(2)-BST film is due to

the inability of the dipole moments in the BST nanograins to orient in the presence of applied field because of the enhanced pinning effect of Ag along the grain boundaries, as the SEM picture (Figure 2c) reveals the absence of large agglomerates of Ag(2)-BST unlike that of the Ag(1)-BST film (Figure 2b).

Figure 4 shows the dielectric loss (tan δ) of BST, Ag(1)-BST and Ag(2)-BST films. At zero bias voltage, tan δ decreases in the order of BST (0.025) > Ag(1)-BST (0.02) > Ag(2)-BST (0.018). The dense microstructure of Ag(2)-BST is the reason for the lowest loss. As the nonagglomerated nanocrystalline Ag(2)-BST grains have more grain boundaries (Figure 2c), and relaxational loss from the grain boundaries is negligible, a reduction in loss characteristics is expected. Moreover, the presence of small amounts of Ag along grain boundaries or interfaces enhances the polarization pinning, and lowers the effective resistance (R) and hence tan δ for a series metal-ceramic configuration of Ag and BST, which lead to low effective dielectric loss. The sharp increase in loss for Ag(1)-BST beyond +4 V may be due to the typical microstructure, which has nonuniform agglomerates that leads to variation in local electric field at high enough applied potential.

Figure 5 shows the XRD patterns of BLT/SiO_2/Si and BLT/TiO_2/Si structure. Single phase BLT could be synthesized on the substrates and no other impurities appear. As shown in the figure, the peak intensity of BLT on SiO_2/Si substrate is smaller than that on the TiO_2/Si substrate. It is implied that the BLT deposited on the TiO_2/Si with the better crystalline structure than that deposited on the SiO_2/Si substrate. The grain size calculated from the XRD result indicated that the BLT deposited on the TiO_2 (43nm) with the smaller grain size than that on the SiO_2 (55nm).

The FESEM images of BLT/SiO_2/Si and BLT/TiO_2/Si are shown in Fig. 6, indicating that the surface morphologies of BLT films depend on the buffer layer on the Si substrate. The chemical composition of BLT was confirmed by the EDX attached with the FE–SEM (not shown here). As shown in Fig. 6 (a), the grain size of BLT film deposited on the SiO_2 buffer layer was 58 nm, while that of BLT film deposited on the TiO_2 buffer layer is 50 nm. Therefore, the BLT deposited on the TiO_2 buffer layer with the better crystalline structure and smaller grain size.

The CV curves (100 kHz) of Pt/BLT/TiO_2/Si structure were shown in Fig.7. As shown in the figure, the memory windows of the structure are increasing from 0.2 to 1.2 V as the gate voltage varied from 2 to 5 V. The dielectric constant of BLT film calculated from the MFIS structure is 430. Therefore, the BLT film with high dielectric constant and modulated memory properties may be appropriate for fabricating MFIS memory devices.

Fig. 8 shows that the I-V measurements of BLT/SiO_2/Si and BLT/TiO_2/Si. The leakage current density of BLT/TiO_2/Si structure is about 2×10^{8} A/cm^2 at 100 kV/cm, while that of BLT/SiO_2/Si structure is about 1.05×10^{7} A/cm^2. The leakage of BLT on the TiO_2 buffer layer is one order of magnitude lower than that on the SiO_2. It is suggested that the better crystalline of BLT reduce the leakage in the structure.

5. Conclusion

In summary, the capacitance and tan δ of Ag-BST films decrease with increasing Ag up to 2 mole % based on a series configuration involving low dielectric interface layers. The dielectric tunability of 1 mole% Ag-BST is better than BST. The 2 mole% Ag-BST has the lowest tan δ at zero bias, which is preserved in the entire sweeping cycle because of its dense microstructure, low relaxational loss, and enhanced polarization pinning along the grain boundaries. Furthermore, the excellent memory characteristics and very low leakage current of BLT/TiO_2/Si structure are the merits for the ferroelectric memory applications.

5. Reference

[1] J. Zhou, L. T. Li, Z. Gui, X. Zhang, and D. J. Barber, Nanostruct. Mater. **8**, 321 (1997).

[2] A. Srivastava, D. Kumar, R. K. Singh, H. Venkataraman, and W. R. Eisenstadt, Phys. Rev. B **61**, 7305 (2000).

[3] S. Y. Chen, C. L. Sun, S. B. Chen, A. Chin, Appl. Phys. Lett. 80, 3168 (2002).

V.

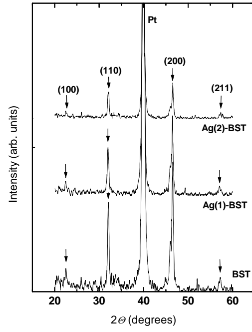

FIG. 1. XRD patterns of BST, Ag(1)-BST and Ag(2)-BST thin films.

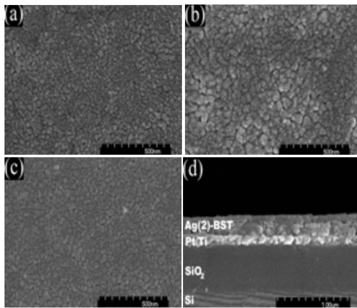

FIG. 2. SEM pictures of surface morphologies of sol-gel-derived (a) BST (b) Ag(1)-BST (c) Ag(2)-BST thin films, and (d) Cross-sectional SEM picture of Ag(2)-BST film (thickness ~ 210 ± 10 nm) on $Pt/Ti/SiO_2/Si$ substrates indicating dense microstructure.

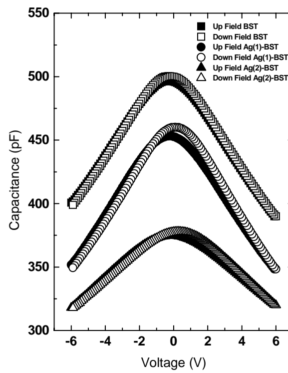

FIG. 3. *C-V* characteristics of BST, Ag(1)-BST and Ag(2)-BST films measured in the range -6 ↔ +6 V.

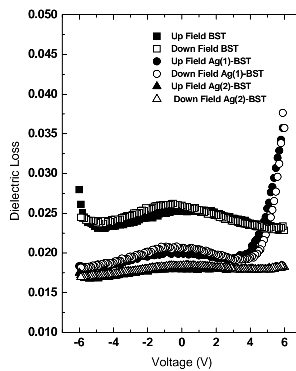

FIG. 4. Dielectric loss (tan δ) characteristics of BST, Ag(1)-BST and Ag(2)-BST measured in the range -6 ↔ +6

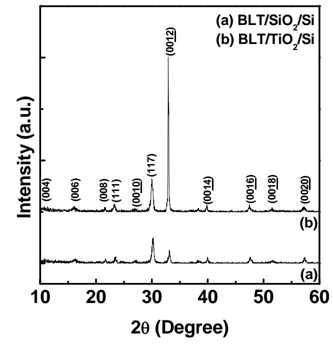

FIG. 5. XRD patterns of $BLT/SiO_2/Si$ and $BLT/TiO_2/Si$

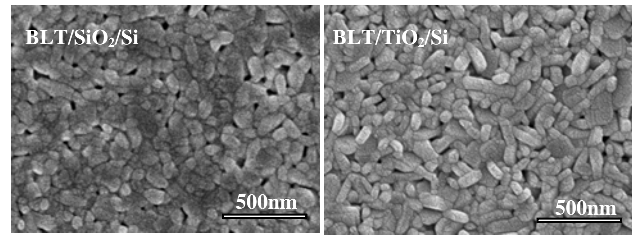

FIG. 6. SEM images of surface morphologies of (a) $BLT/SiO_2/Si$ and $BLT/TiO_2/Si$

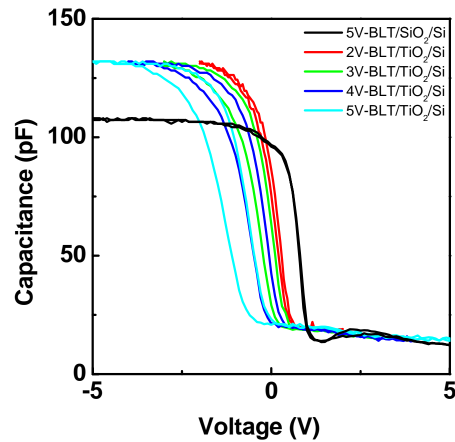

FIG. 7. *C-V* characteristics of $BLT/TiO_2/Si$ structure.

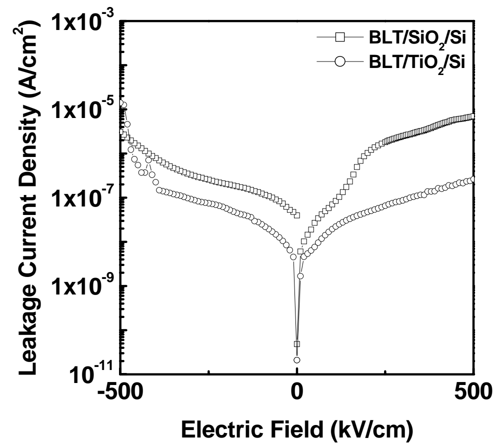

FIG. 8 *I-V* characteristics of $BLT/SiO_2/Si$ and $BLT/TiO_2/Si$ structure.